Pergamon

Int. J. Heat Mass Transfer. Vol. 39, No. 14, pp. 3045–3055, 1996

0017-9310/96 $15.00 + 0.00

0017-9310(95)00380-0

Experiments on heat transfer of smooth and swirl tubes under one-sided heating conditions

MASANORI ARAKI, MASURO OGAWA, TOMOAKI KUNUGI, KAZUYOSHI SATOH and SATOSHI SUZUKI

Department of Fusion Engineering Research, Naka-Fusion Research Establishment, Japan Atomic Energy Research Institute, 801-1, Naka-machi, Naka-gun, Ibaraki-ken, 311-01 Japan

(*Received* 21 *April* 1995; *and in final form* 28 *July* 1995)

Abstract—To design the divertor plate for the next generation fusion machines which is subjected to high heat loads on its one side by the plasma, it is essential to evaluate performances of heat transfer efficiency. However there is little in the literature for predicting of heat transfer coefficients under such one-sided heating conditions. To establish the heat transfer correlation for water under one-sided heating conditions, the authors have performed heat transfer experiments on smooth circular and swirl tubes in the regions from non-boiling to high subcooled partial nucleate boiling. Based on the experimental results, it is confirmed that the existing heat transfer correlations can be applicable at the non-boiling region. For the subcooled partial nucleate boiling region, they cannot be available so that a new heat transfer correlation has been proposed under one-sided heating conditions. Copyright © 1996 Elsevier Science Ltd.

1. INTRODUCTION

The plasma facing component for the next generation fusion machines such as an International Thermonuclear Experimental Reactor (ITER) is exposed to severe steady state heat loads on its one side. In particular, the surface heat flux of the divertor plate is estimated to be 15–30 MW m^{-2} in ITER-CDA (ITER Conceptual Design Activities) [1]. Since the nucleate boiling of the deionized water partially occurs in the cooling tube of the divertor plate, a tube with a twist tape for enhancement on heat transfer and critical heat flux, namely swirl tube, is applied as the cooling tube. To develop the divertor plates, R&D including manufacturing and testing of the divertor plate have intensively been performed in the world [2–5]. On the other hand, some ideas of the surface heat flux reduction are proposed for the divertor plate [6–8]; in ITER-EDA, a dynamic gas target divertor concept is introduced [8]. When this divertor concept effectively works for reducing the surface heat flux, it will give the surface heat flux around 5 MW m^{-2} on the divertor plate. However uncertainties of this concept such as the possibility of the pressure reduction as high as a magnitude of four between the divertor region and the main plasma are still retained. Therefore, it is necessary to develop the divertor plate which withstands a high heat flux of more than 15 MW m^{-2} for steady-state heating conditions.

To design the divertor plate for ITER, it is essential to evaluate the heat transfer coefficients under one-sided heating conditions. Up to now, studies on heat transfer characterization at uniform heating condition have been done around the world [9–14]. However, no confirmation has been recorded on whether or not these existing heat transfer correlations are applicable for one-sided heating conditions. Kim *et al.* [15] and Milola *et al.* [16] tried to evaluate non uniform heat transfer of the swirl tube in both non-boiling and subcooled boiling regions. Their studies, however, were included an assumption that the heat transfer coefficient is independent on inner wall flux variation. Because of creating the swirl flow in the tube, it will be difficult to determine the heat transfer coefficient along the circumference and the flow direction in the swirl tube. On the other hand, Schlosser *et al.* [17] proposed a heat transfer correlation for one-sided heating conditions based on the existing correlation at uniform heating condition. However, they also informed that further efforts for developing the precise heat transfer correlation are necessary due to lack of data.

Therefore, heat transfer experiments of the smooth circular tube and the swirl tube have been performed to evaluate heat transfer characteristics under one-sided heating conditions in regions from non-boiling to the subcooled partial nucleate boiling.

2. EXPERIMENTAL SET-UP

In the experiments, Particle Beam Engineering Test Facility [18], namely PBEF, was used. PBEF, which consists of vacuum chambers, an ion source, a high voltage power supply system, a cooling water system, a vacuum pumping system, a control system, and a

NOMENCLATURE

G	mass flow rate [kg m^{-2} s^{-1}]
k	effective variable for forced convection heat transfer
p	local pressure [MPa]
q	heat flux [MW m^{-2}]
T	local temperature [°C]
X	ratio normalized by θ^*, $(=\theta/\theta^*)$.

Greek symbols

γ	fraction of total heated length measured from inlet
θ	angle from top of the tube [degree]
θ^*	angle at the boiling initiation point measured from top of the tube [degree].

Subscripts

bo	nucleate boiling
con	forced convection
exp	experiment value
in	inlet
out	outlet
sat	saturation
wall	inside wall.

data acquisition system as shown in Fig. 1, can deliver the intense hydrogen ion beams up to 5 MW for durations for 0.01 to 10 s. Figure 2 shows a schematic of the main vacuum chamber of PBEF. This chamber made of stainless steel has many ports for installing the measuring equipment and data acquisition system. Major dimensions of the vacuum chamber are 1.5 m diameter and 5.0 m high. At top of the chamber, an ion source is mounted as a heat source. This ion source has originally been developed for neutral beam injectors of JT-60. As seen in Fig. 2, the ion source consists of a source plasma generator and an acceleration grid system. At the plasma generator, hydrogen source plasma is produced by arc discharge process using hair-pin-shaped tungsten filaments. Only hydrogen ions are stably extracted by the acceleration grid system at beam energies ranging from 30 to 100 keV with the beam current up to 50 A which corresponds to the beam current density of up to 4000 A/m^2.

There are three test sections in the chamber, i.e. two test sections with forced water cooling lines and one test bed with a remotely handled system. In this experiment, test sample was set in the vacuum chamber as shown in Fig. 2 to form a horizontal flow. At bottom of the chamber, a passively cooled ion dump which consists of many array of copper blocks with cooling tubes is installed to stop whole particle beams. In the heat transfer experiments, an additional ion dump is mounted to handle intense hydrogen ion beams at steady state because an area of the intense ion beams is very wide compared with the test sample size. The additional ion dump, an actively cooled ion dump, consists of 16 array of swirl tubes with an external fin.

PBEF water cooling system consists of de-ionized water cooling loops at a pressure of up to 1.5 MPa and a heat exchanger loop. De-ionized water is produced with an ion purification system to keep its electric resistance more than 1 MΩ cm^{-1}. As shown in Fig. 1, one water cooling loop is used for all beamline components such as the ion source, ion dumps and test sections, and the other loop is used for the power supply system. In the cooling loop for the beamline, de-ionized water is pumped up to 1.5 MPa with a circulating pump and cools the beamline components. High pressurized water up to 2.0 MPa is also available for the actively cooled ion dump and the test sections using an additional pump unit. Measured maximum pressure and flow rate (flow velocity) at the inlet of the test sample were limited to be 1.6 MPa and 1.25 kg s^{-1} ($\sim$16 m s^{-1}), respectively, due to narrow connection pipes and joints. Temperature control of the de-ionized water is also temporarily possible at the range of up to 100°C to evaluate an effect of heat transfer on different degree of subcooling. In this case, inlet water pressure is limited to be up to 1 MPa due to weak heater unit used.

For this experiment, data logging system which has a sampling speed as fast as 1.0 ms (32 channel)$^{-1}$, and an i.r. camera which has a sampling speed of 30 ms image^{-1} were mainly used as shown in Figs. 1 and 2. In particular, the data logging system consists of two parts, i.e. a data logging part with 32-channel high speed amplifiers for various types of signals from thermocouples, flow meter and pressure gauges, and data analysing part. In the data analysing equipment, all data are analysed using original software developed for this experiment after recording them in its hard disk memory.

3. TEST SAMPLES

A circular smooth tube as a basic configuration and circular swirl tube were fabricated in this experiment. Figure 3 shows a schematic of the test sample. Dimensions of the test samples are 15 mm o.d., 10 mm i.d., 474 mm in length (length of test section; 400 mm). Thermocouples were bonded into the test sample at a pitch circle diameter of 13.0 mm$\pm$0.1 mm which corresponds to a depth of 1.0 mm$\pm$0.05 mm from the surface. The specification of each thermocouple is high grade type K sheathed with outer diameter of 0.5 mm made of stainless steel (SS316L), which has a

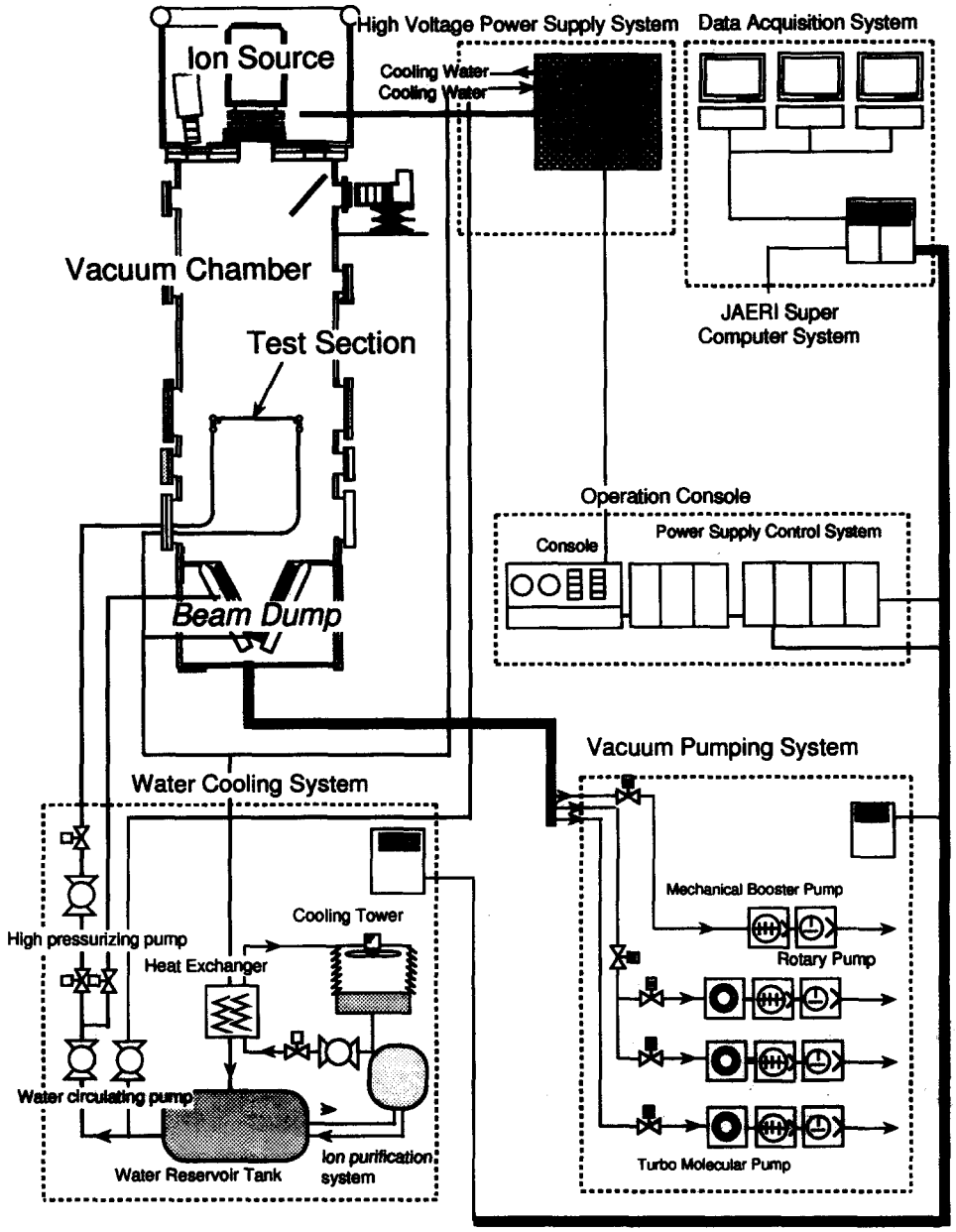

Fig. 1. System diagram of JAERI PBEF.

response time of several ms and an accuracy of $\pm 0.4\%$ for full scale. To measure temperature profile along the flow direction, five thermocouples are used. On the other hand, thermocouple position for temperature measurement along the circumference of the test sample was determined from the results of the previous experiments [18]. In the regions of the tube surface from zero (top of the test sample) to 180° (bottom of the test sample), nine thermocouples are circumferentially bonded into the test sample with every angle of 22.5° at point "d" as shown in Fig. 3. On the other side, four thermocouples are also bonded into the test sample with every 22.5° from 11.25° to 78.75° to interpolate the temperature data at the heating side.

The test samples were made of oxygen free high conductivity copper (OFHC-Cu) because its thermal and mechanical properties are well-known. A silver brazing filler metal with a melting temperature around 720°C which consists of 44–46% of silver, 29–31% copper and 23–27% zinc was used for matching the thermal properties of OFHC-Cu bulk material.

The thermal deformation as large as 20 mm at the center region induced by temperature gradient between top and rear of the test sample was confirmed in the previous experiments [18, 19]. To minimize the

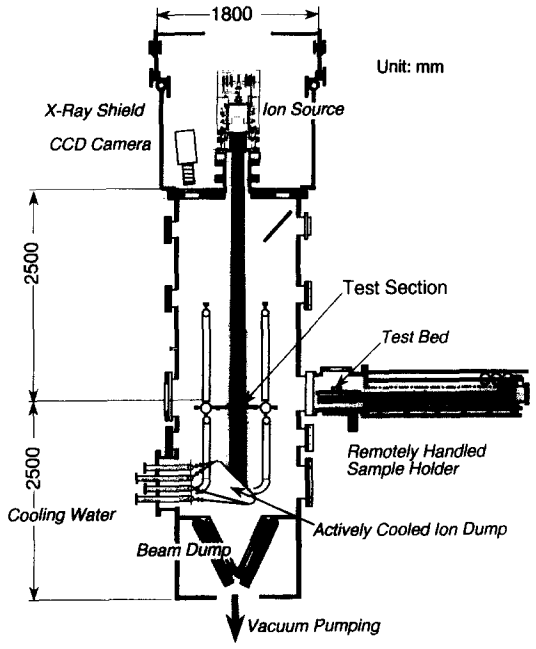

Fig. 2. Schematic of JAERI Particle Beam Engineering Facility.

thermal elastic and plastic deformations during heating, a plate made of OFHC-Cu with a thickness of 4.8 mm and depth of 15 mm was brazed to the test sample at rear side (bottom of the tube).

For swirl tube, a thin tape with a thickness of 0.35 mm made of Inconnel-625 was twisted, and then the twisted tape was inserted and fixed to a smooth tube inner wall by cold working process. A tape twist ratio of 3.0 which is defined as a number of internal diameters for 180° of twist was selected based on the previous experiments [18]. The binding force between a twisted tape and an inside wall of the tube, which was amount of the tensile force divided by the tape insertion length, was more than 600 N m^{-1} at temperatures in ranges from 20 to 400°. This value is enough to be fit for a water pressure of up to 4 MPa. Furthermore, even if the binding force is reduced, sleeves which protrude from the inside wall at both ends of the tube will prevent the twisted tape from slipping off. After fabricating the swirl tube, 0.5 mm diameter thermocouples were bonded at the identical positions as the smooth tube.

It is also essential to measure the inlet and outlet water pressure and temperature for the determination of the degree of subcooling and pressure drop. A manifold pipe for test sample with pressure measurement ports was also fabricated and set at both ends of the test sample. For this purpose, sensors with a diaphragm were used. This sensor has specifications that permissible measurable pressure and temperature ranges are from 0 to 5 MPa within an error of ±3% with respect to full scale and from RT to 200°C, respectively.

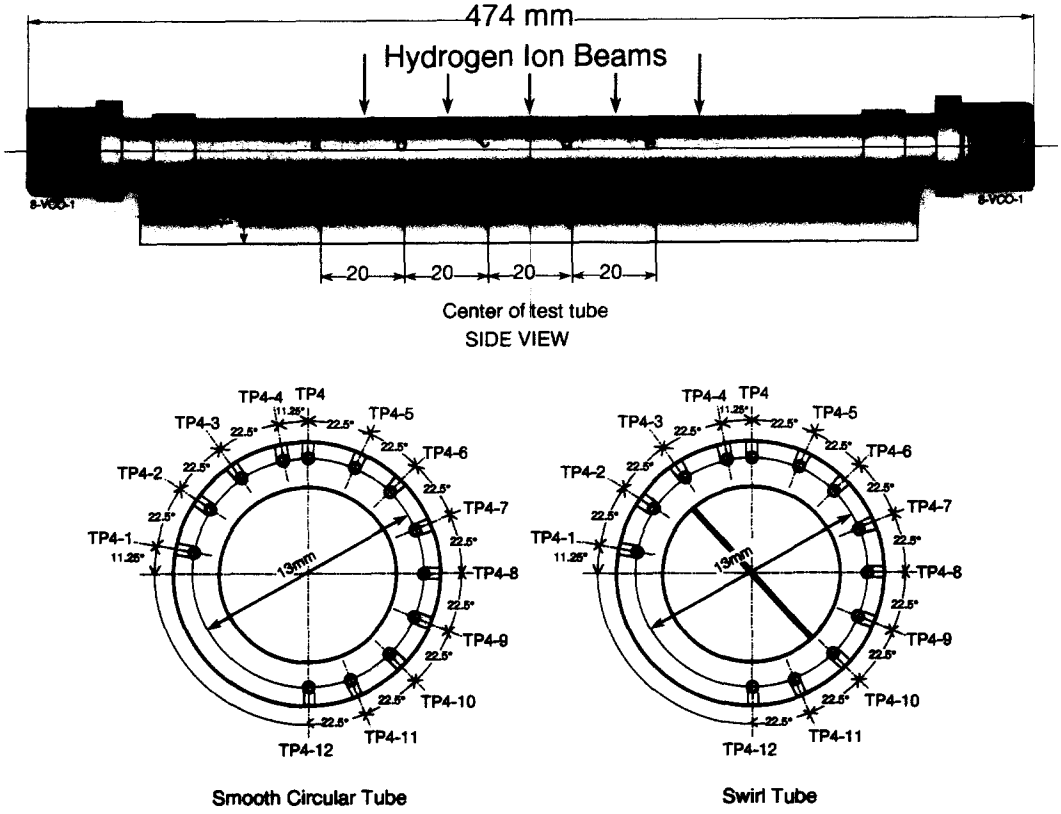

Fig. 3. Schematic of the test sample for heat transfer experiment.

4. EXPERIMENTS

4.1. *Surface heat flux measurements*

For measuring the surface heat flux at the test sample position, two different calorimetries are applied. One is a multi-channel calorimeter, and the other is a water calorimetry. The multi-channel line calorimeter consists of 11 cylindrical copper chips with each surface area of 2 cm^2 for volume of 1 cm^3. One high grade K-type thermocouple with a sheath diameter of 1.0 mm is bonded to each copper chip in the rear side with a depth of 2.0 mm. To obtain almost adiabatic temperature rise of the cylindrical copper chip during heating, each copper chip is fixed by a small cylindrical stud bolt made of stainless steel with a diameter of 3 mm. Therefore, heat loss through the bolt can be minimized due to its low thermal conductivity compared with copper and be calculated to be a few per cent (approx. 3%) of the total deposited power. From quasi-adiabatic temperature rises of 11 copper chips in line, surface heat fluxes and a beam profile can be determined [19]. Figure 4 shows typical surface heat flux distributions at the test sample position measured with the multi-channel calorimeter for different beam conditions. The abscissa is the position along the flow direction where zero position corresponds to the center of the test sample. Each symbol, ○, □, ◇, △ and × in the figure shows the surface heat flux at different beam conditions. Heat flux profile in the flow direction is almost Gaussian with a full width at half maximum (FWHM) of around 120 mm for all beam extraction conditions because of the beam perveance matched operation. On the other hand, deposited heat flux distributions in the cross sectional direction of the test sample have been measured and confirmed to be almost flat within a width of ±20 mm. In the experiment, the surface heat flux distribution along the circumference of the test sample is assumed to be cosine profile because of a small reflection loss (approx. 2%) of the hydrogen ion beams.

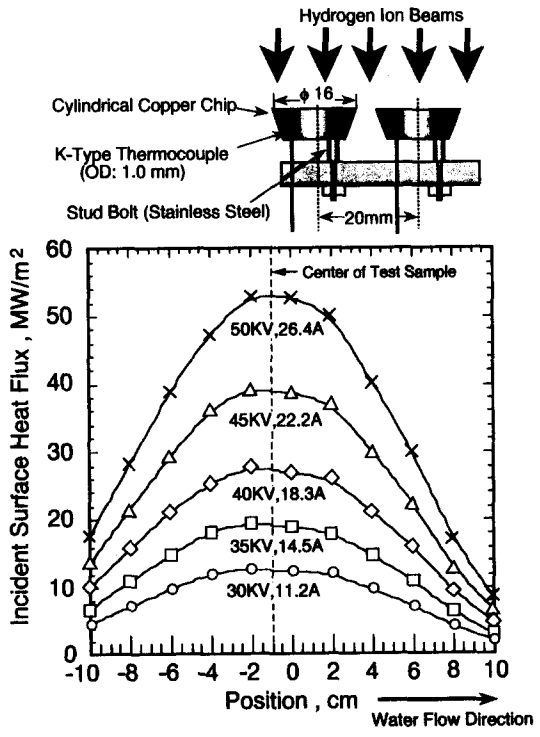

Fig. 4. Surface heat flux distributions at the test sample position. It is noted that the test sample was set at 1.0 cm upstream from the center of the PBEF chamber for fitting it at the beam center.

The other calorimetry, water calorimetry, has been carried out in order to cross-check the multi-channel calorimetry described above and to evaluate local water temperature. From the water calorimetry, only total absorbed power into the water is measured. Since the surface heat flux distribution is already measured by the multi-channel calorimetry, total absorbed power into the water should be given as a sum of the absorbed heat fluxes in the test sample [18]. Therefore, the surface heat flux can be determined. It is confirmed that the surface heat fluxes by the water calorimetry are very consistent with those measured by multi-channel calorimetry within an error of ±10%.

4.2. *Experimental conditions*

To evaluate heat transfer coefficients and an effect of heat transfer on different degree of subcooling under one-sided heating conditions for the ITER divertor plate, experimental conditions are selected as follows:

Flow velocity;	4.2–16 m s^{-1}
Local pressure;	0.5–1.3 MPa
Surface heat flux;	2.0 ~ burnout MW m^{-2}
Inlet water temperature, °C;	20–80°C
Beam duration;	up to 2.0 s.

The experimental procedure is as follows; at first, water flow velocity and local pressure were adjusted by the inlet and outlet slot valves. Keeping the water flow condition, hydrogen ion beams with a low peak surface heat flux around 2 MW m^{-2} were exposed to the test sample until all thermocouples reached steady state condition. Subsequently, the surface heat flux was increased with a small step around 2 MW m^{-2} up to burnout. As the preliminary experiment, it was confirmed that beam duration around 1.0 s was enough to obtain steady-state condition. Detail will be discussed in the next section.

5. EXPERIMENTAL RESULTS

To turn around the experiments, pulse heating experiments have been done. A pulse duration of 1.0 s was selected to reach steady-state heating condition. Figure 5 shows typical temperature response measured with thermocouples. From Fig. 5(a), it is clearly seen that all temperature signals from thermocouples reach steady-state condition at a pulse duration of up

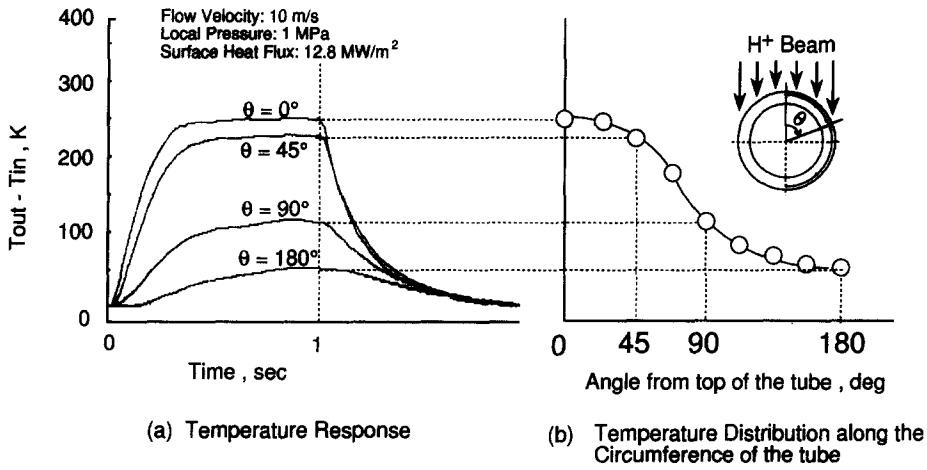

Fig. 5. Typical temperature responses of thermocouples bonded in the test sample.

to 1.0 s. A temperature distribution along the circumference of the test sample after 1.0 s beam-on is shown in Fig. 5(b). At a surface heat flux of 12.8 MW m^{-2}, at which nucleate boiling is formed in a region at the top of $\pm$ around 60°, temperature difference between top and bottom of the smooth tube sample reaches as high as 200 K. Even if such a high temperature gradient is observed during the experiments, maximum thermal deformation at the center of the test sample was confirmed to be less than 2.0 mm.

The absorbed heat at the tube outer surface mainly moves into the coolant, while some fraction of the absorbed heat diffuses to the circumference and the flow direction of the test sample tube. For temperature distribution in the flow direction under the identical heating and cooling conditions shown in Fig. 5, it is found that a fraction of heat absorption at a position of TP-4 slightly diffuses to the flow direction. However this fraction is estimated to be around 3.5% compared with heat conduction to the circumference. Therefore, the fraction of heat loss in the flow direction is not considered in the analyses described in next section. All experimental data are presented in ref. [20] as a data book.

6. HEAT TRANSFER EVALUATIONS

Based on the temperature distributions obtained in the experiments, heat transfer coefficients can be calculated. Figure 6 shows the evaluation procedure for the prediction of heat transfer coefficients under one-sided heating conditions. It is in two parts as follows: (1) finite element thermal analyses using the existing heat transfer correlations are performed under the experimental conditions. From the analyses, temperatures in the test sample and inside heat flux and heat transfer coefficient can be obtained. Subsequently, circumferential temperature distribution at the thermocouple position is compared with the experimental results to evaluate the applicability of the existing correlations to one-sided heating conditions. (2) Based on the experimental data, inverse analyses of thermal conduction problems are used to estimate inside distributions on heat flux, temperature and on heat transfer coefficient by analysing the surface heat flux distribution and temperature distribution at the thermocouple position. In this paper, the latter issue is presented since the former issue was previously reported [19, 20].

6.1. *Inverse analyses of heat conduction problems*

Two-dimensional inverse analyses of heat conduction problems have been done using the experimental data to determine heat transfer coefficient under one-sided heating conditions. Analytical procedure and model are shown in Fig. 7. Based on the analyses, the inside heat flux and temperature are obtained.

To establish inverse analysis code of heat conduction problems, a boundary element method (BEM) was applied [21]. This analytical method is to solve linear integral equations obtained by the following process: (1) at first, a partial differential equation of the boundary problem which has unique solution is translated into integral equation on the boundary applying Green theorem; (2) the boundary is divided into boundary elements defined by linear equations.

Although an infinitely small distance, DR, as shown in Fig. 7 (2) can arbitrarily be defined, it should be optimized to obtain accurate solution. With decreasing distance DR, accurate solution by the inverse analysis of heat conduction problems would be obtained: however, the number of the iteration processes also increases, resulting in increase of sum of errors induced by the analytical processes. On the other hand, with increasing the number of fine boundaries, accurate solution by normal heat conduction analysis would also be obtained, while the number of unknown values also increases. Subsequently, the sum of errors induced by processes of inverse analyses of heat conduction problems should increase. Therefore,

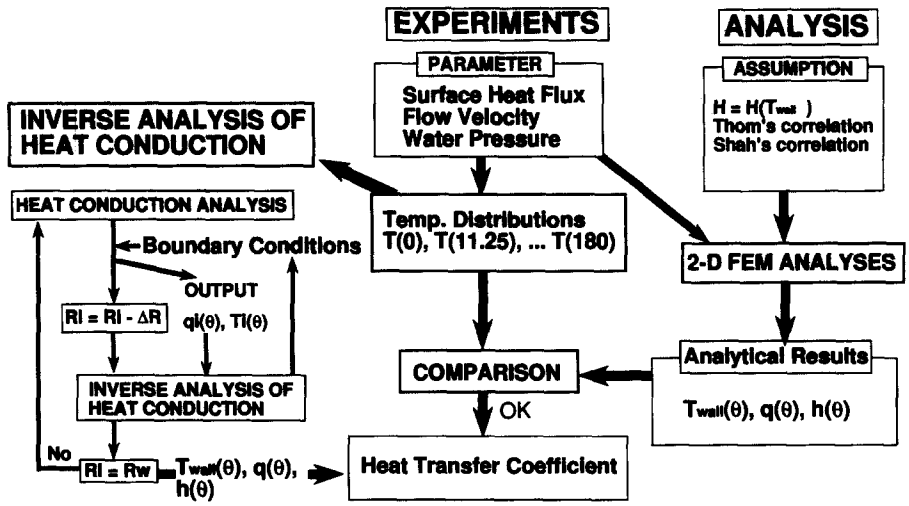

Fig. 6. Evaluation procedure for the prediction of heat transfer coefficients.

the optimum values for the number of fine boundaries and for an infinitely small distance DR should be found. After optimizing them, the distance DR and the number of fine boundaries were selected to be 0.1 mm, 64 for boundary along the circumference, and 16 in radial in the analyses. The applicability of this code was confirmed by simple bench mark analysis within an error of a few per cent (<1.5%).

6.2. *Heat transfer under one-sided heating conditions*

6.2.1. *Heat transfer at non-boiling region.* For smooth tube test sample, measured temperature distribution shows relatively good agreement with Dittus–Boelter equation [9] taking account of the ratio of viscosity at bulk temperature to that at the wall temperature in non-boiling region. Consequently,

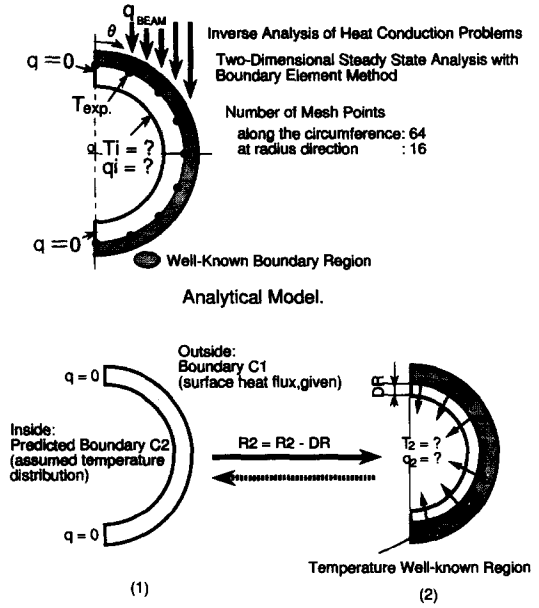

Fig. 7. Conceptual diagram in inverse analysis of heat conduction problems.

Nusselt numbers obtained in the experiments were compared with the above equations. Figure 8(a) shows Nusselt number as a function of Reynolds number. It seems that experimental Nusselt number is slightly deviated from an original Dittus–Boelter equation, but experimental data match to Dittus–Boelter equation with a viscosity factor.

For swirl tube test sample, measured temperature distribution also shows relatively good agreement with Gambill equation [11] applied a viscosity factor at non-boiling region. Figure 8(b) shows the plots of Nusselt number in the experiments. It is clearly seen that Gambill equation with a viscosity factor gives better prediction than the original one.

At the non-boiling region, no differences in heat transfer coefficients between uniform and one-sided heating conditions have been confirmed in the experiments due to low surface heat fluxes, low heat transfer coefficients, high conductivity copper and thicker wall test samples.

6.2.2. *Heat transfer at subcooled partial nucleate boiling region.* Before starting the inverse analysis of heat conduction, preliminary normal thermal calculations using the existing heat transfer correlations described above were performed to briefly evaluate their applicability for one-sided heating conditions. The result showed that the existing correlations could not predict the experimental results [19]. Therefore, wall heat flux and wall temperature are evaluated as a function of the position in accordance with the evaluation procedure as shown in Figs. 6 and 7. Figures 9(a) and (b) show typical inside wall temperature and heat flux distributions along the circumference of the smooth tube. In these figures, it is noted that a nucleate boiling initiation point depends on the surface heat flux and that with increasing the surface heat flux the wall heat flux at the top of the test sample increases drastically due to enlarging the heat transfer efficiency caused by nucleate boiling. On the other hand, almost similar temperature difference and wall

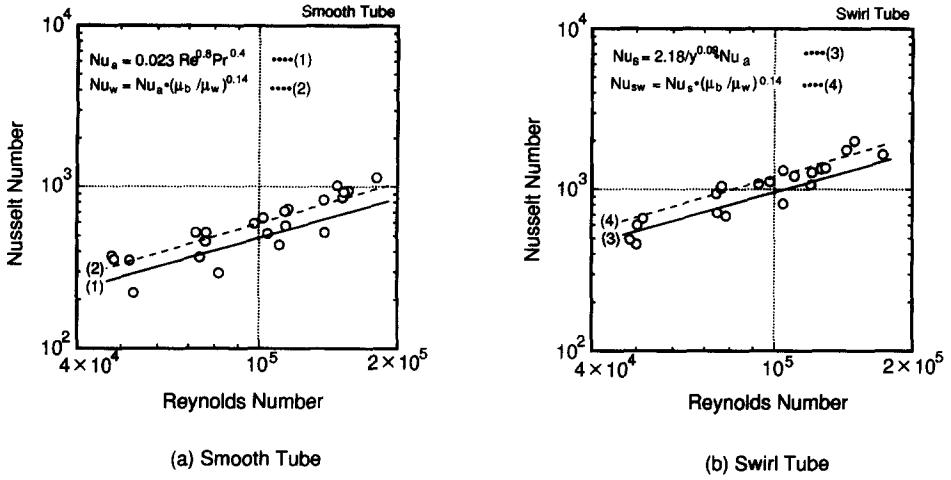

Fig. 8. Heat transfer characteristics at non-boiling region.

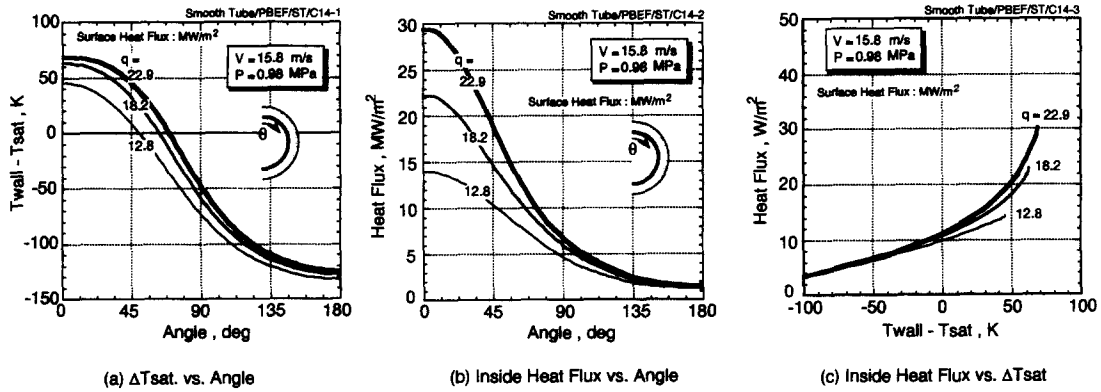

Fig. 9. Numerical results from the inverse analyses of heat conduction problems.

heat flux are confirmed at the rear of the test sample even if the surface heat flux changed from 12.8 to 22.9 MW m^{-2}. To evaluate heat transfer efficiency, a relation between the inside heat flux and degree of superheating, $(T_{wall} - T_{sat})$, is necessary. Therefore, the obtained wall heat fluxes can be replotted as a function of degree of superheating for different surface heat fluxes as shown in Fig. 9(c). In the figure, the absorbed surface heat flux in present experimental conditions is also indicated. A peaking factor which is defined by a ratio of the absorbed surface heat flux to the wall heat flux increases with the absorbed heat flux, but does not reach a ratio of o.d./i.d. which was applied in order to estimate the wall heat flux of plasma facing components such as the divertor plate [1]. The wall heat flux increases nearly linear at non-boiling region, while it increases non-linear at developing nucleate boiling region. However, almost linear wall heat flux was obtained at the absorbed heat flux of 12.8 MW m^{-2} because the heat transfer coefficient at non-boiling regime should dominate at that condition. Figures 10 and 11 also show inside heat flux distributions for different inlet water temperatures at constant values of flow velocity, local water pressure, and surface heat flux for the smooth and the swirl tubes, respectively. Particularly, from Fig. 10 it is found that the inlet water temperature corresponding to the subcooling does not affect the wall heat flux at the top of the test sample in the nucleate boiling region. In Figs. 9(c), 10

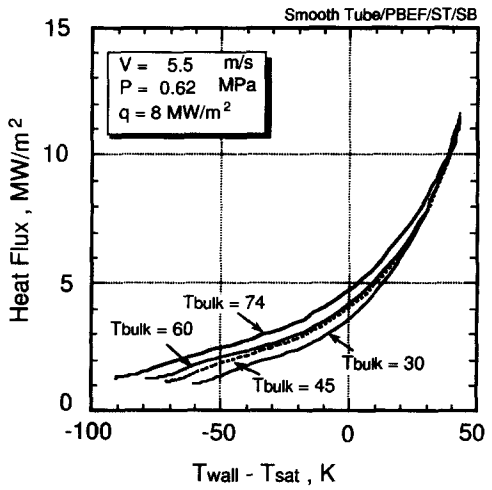

Fig. 10. Relation between superheat and inside heat flux at the inner wall of smooth tube.

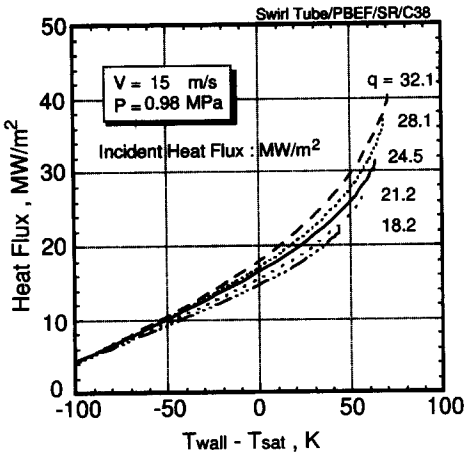

Fig. 11. Relations between superheat and inside heat flux at the inner wall of swirl tube.

and 11, a right end point in each curve corresponds to an inside point at the top of the test sample ($\theta = 0°$). At the absorbed surface heat flux of 12.8 MW m^{-2} for the smooth tube, the inside wall heat flux is calculated to be around 14.2 MW $^{-2}$. A peaking factor, which is defined by a ratio of the inside heat flux to the surface heat flux, is about 1.11. With increasing the surface heat flux, the peaking factor increases due to developing the partial nucleate boiling. To evaluate heat transfer coefficients at nucleate boiling region, data at point $\theta = 0°$ are plotted as a function of superheat in Fig. 12. Symbols ○, ●, △ and ▲ indicate heat fluxes at local pressure up to 1.0 MPa and at local pressure higher than 1.0 MPa for the smooth tube test sample, and at local pressure up to 1.0 MPa and at local pressure higher than 1.0 MPa for the swirl tube test sample, respectively. Data from the existing heat transfer correlations are also presented in the figure. It is clearly seen that the existing heat transfer correlations can not predict inside heat fluxes at high superheat region because the superheat range in their experiments is small compared with the present experiment. Therefore, it may be out of range for the evaluation of heat transfer coefficients in relatively high superheat region. On the other hand, it is found that all experimental data for both test samples can be arranged in a curve as shown in Fig. 12. From the precise data analyses, we have proposed a new heat transfer correlation at the subcooled partial nucleate boiling region as follows,

$$T_{wall} - T_{sat} = 25.72 \times q^{1/3} / \exp(p/8.6) \qquad (1)$$

where the range of application for equation (1) is as follows: $T_{wall} - T_{sat}$ = 40–90 K, p = 0.5–1.6 MPa; T = 30–80°C; q < 60 MW m^{-2}. As seen in Fig. 12, the correlation can predict the wall heat fluxes within an error of ±15% at nucleate boiling region under one-sided heating conditions.

6.1.3. *Heat transfer along the circumference of the tube.* Because of one-sided heating conditions, inside wall temperatures along the circumference of the test sample widely distribute, resulting in wide distributions of heat transfer coefficients from non-boiling to nucleate boiling regions. Therefore, heat transfer coefficients at transient to nucleate boiling region should be evaluated. Figure 13 shows inside heat fluxes obtained by the above analytical processes using the experimental data for the smooth tube. The abscissa indicates superheat. Symbols ○ and △ also show inside heat fluxes at surface heat fluxes of 18.2 and 22.9 MW m^{-2}, respectively. An area formed nucleate boiling strongly depends on its surface heat flux so that it gives different inside heat flux dis-

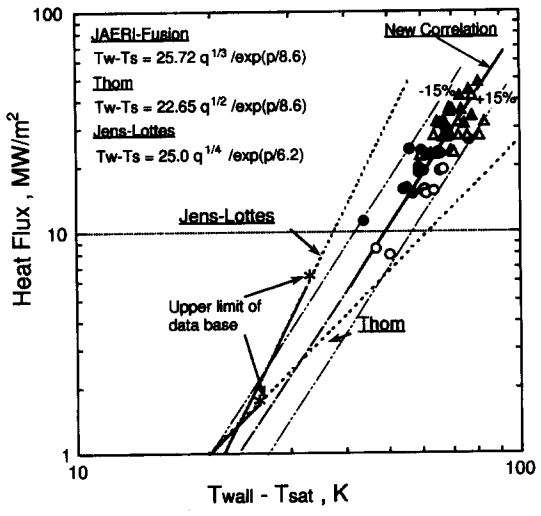

Fig. 12. Comparison of experimental data and the existing heat transfer correlations at nucleate boiling region. In the figure, symbols ●, ○, ▲ and △ indicate the values of heat fluxes at local pressure up to 1.0 MPa and at local pressure higher than 1.0 MPa for smooth tube, and at local pressure up to 1.0 MPa and at local pressure higher than 1.0 MPa for swirl tube, respectively.

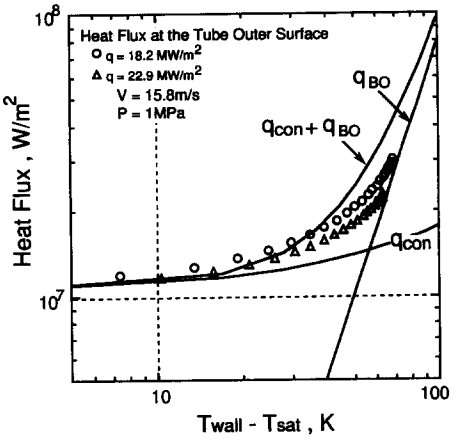

Fig. 13. Inside heat fluxes of the smooth tube in the subcooled partial nucleate boiling region. In figure, symbols ○ and △ indicate inside heat fluxes at surface heat fluxes of 18.2 and 22.9 MW m^{-2}, respectively. These inside heat fluxes are obtained by the analytical processes which consist of normal and inverse analyses of heat conduction problems.

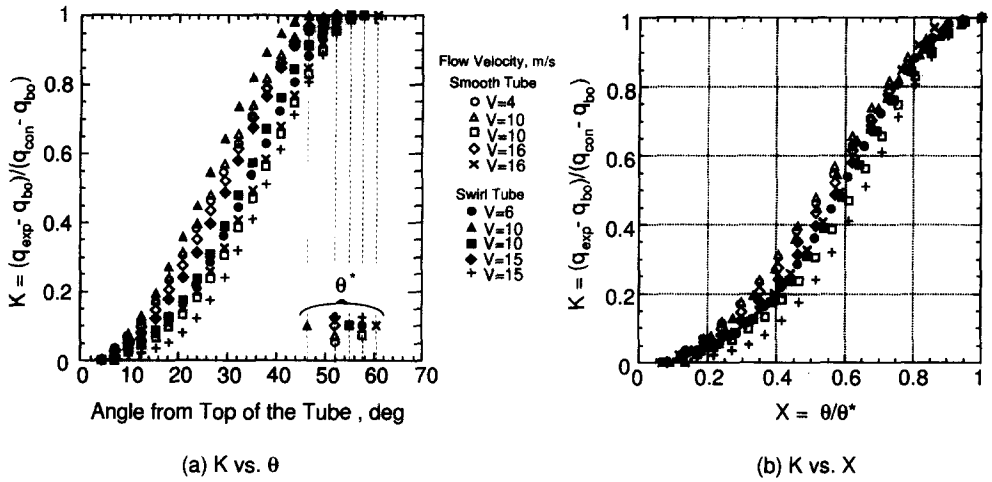

(a) K vs. θ (b) K vs. X

Fig. 14. A relation between k and angle. In the figure, θ^* indicates an angle of boiling initiation point for different flow velocities. The abscissa in (b) is ratio normalized by θ^* in which $x = 1$ means the boiling initiation point.

tributions even if the same superheat. It results that heat transfer under one-sided heating conditions can be indicated as a combination of the effects in non-boiling and nucleate boiling as follows,

$$q = k \times q_{con} + (1-k)q_{bo} \tag{2}$$

where k, q_{con} and q_{bo} are effective variables for forced convection heat transfer as a function of a circumferential angle, heat flux for forced convection flow and heat flux for boiling, respectively.

Figures 14(a) shows measured k-values which are obtained as solutions that satisfy with $q = q_{exp}$. In the figure, the abscissa is an angle from top of the test samples. Each symbol indicates k-value for different cooling conditions in both cooling geometry as shown in the figure. It seems that there is no relationship between data for different cooling conditions. This reason is attributed to different nucleate boiling initiation points, i.e. k reaches to unity at different angles θ^*. Therefore, it is necessary to arrange k-values as a function of the specified angle normalized by θ^*. Figure 14(b) shows replotted k-values as a function of θ/θ^*. Figure 15 also shows k-values obtained at constant cooling and heating conditions for the inlet water temperatures ranging from 30 to 74°C. From these figures, it is clearly seen that under one-sided heating conditions a fraction of forced convection heat transfer which is 1 at the nucleate boiling initiation point decreases with increasing θ/θ^* and reaches to zero at $\theta/\theta^* = 0.1$, and that effects of heat transfer on the subcooling can be indicated only as an effect on forced convection heat transfer. Furthermore, relationship between k-value and θ/θ^* seems to roughly be indicated as a sine curve as follows,

$$k = (\sin(180X - 90) + 1)/2 \tag{3}$$

where, $X = \theta/\theta^*$.

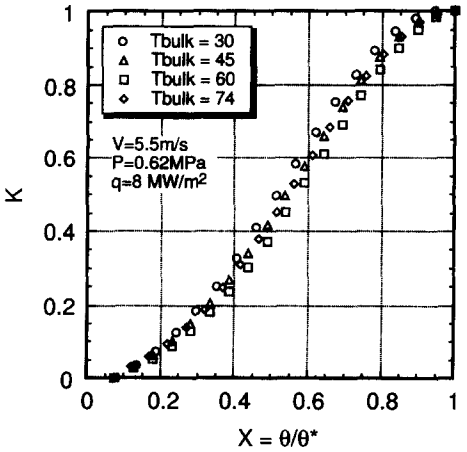

Fig. 15. A relation between k and ratio normalized by θ^*.

7. DISCUSSION

To determine heat transfer coefficients under one-sided heating conditions, it is essential to provide the nucleate boiling initiation point. The determination of the boiling initiation point, however, can be available by applying the following process; at first, rough boiling initiation point is estimated by the thermal analysis using the moderate constant heat transfer coefficient and subsequently thermal analyses using the previous result are continued until converging the solution. Easy analysis is also roughly available to use Bergles–Rohsenow equation [12] at transient to nucleate boiling region instead of the above process. In the preliminary results, it was confirmed that this approach can give us relatively reasonable heat transfer coefficients at transient to nucleate boiling because of dominating the nucleate boiling heat transfer compared with non-boiling one. In an area that is still estimated at non-boiling region, it should be noted that this prediction gives little bit lower heat transfer

coefficients than that predicted by the present correlation.

The present heat transfer correlation was compared with correlations proposed by Thom and Jens-Lottes, and the results showed that the existing correlations based on uniform heating condition can not be used at highly subcooled partial nucleate boiling region such as the ITER divertor conditions described above. On the other hand, Schlosser *et al.* [17] and Yin *et al.* [22] recently proposed the following heat transfer correlations.

Schlosser *et al.*:

$$T_{wall} - T_{sat} = 22.65 \times q^{0.357} / \exp(p/8.6), \quad (4)$$

range: $p = 1.2$–3.6 MPa, $q < 60$ MW m^{-2}
Yin *et al.*:

$$T_{wall} - T_{sat} = 7.195 \times q \times \gamma^{1.82} / P_{out}^{0.072} \quad (5)$$

range: $P_{out} = 1.0$–12 MPa, $T_{in} = 30$–150°C, $q = 0$–16 MW m^{-2}, $\gamma = 0.7$–1.0.

In a comparison of their correlations with the present correlation, it is confirmed that a correlation proposed by Schlosser *et al.* shows relatively good agreement with the present correlation except at lower superheat region. This is from the fact that the fraction of boiling heat transfer is estimated with a large error because non-boiling heat transfer dominates the overall heat transfer efficients at that condition. On the other hand, a large discrepancy between a correlation proposed by Yin *et al.* and the present correlation is observed. This reason, however is not clear yet, would be attributable mainly to different experimental conditions which Yin *et al.* performed the experiment under uniform heating condition and different heated length at low heat flux.

Acknowledgements—The authors would wish to thank Y. Ohara, M. Akiba and the members of NBI Heating Laboratory for their valuable discussions, comments and supports on the experiments, and thank W. Hashimoto of Nikon Systems Co., Ltd for his continuous support with the calculations. They also would like to acknowledge Y. Tanaka, S. Shimamoto, T. Nagashima and M. Ohta for their support and encouragement.

REFERENCES

1. T. Kuroda, G. Vieider, M. Akiba, A. B. Antipenkov, M. Arki *et al.*, ITER Documentation Series No. 30, IAEA, Vienna (1991).
2. M. Araki, M. Akiba, M. Dairaku, K. Iida, H. Ise, M. Seki, S. Suzuki and K. Yokoyama, Thermal response of bonded CFC/OFHC-Cu divertor mock-ups for fusion experimental reactors under large numbers of cyclic high heat loads, *J. Nucl. Sci. Technol.* **29**(9), 901–908 (1992); and also see S. Suzuki, M. Akiba, M. Araki, K. Satoh, K. Yokoyama, M. Dairaku, High heat flux experiments of saddle type divertor module, *J. Nucl. Mater.* 212–215, 1365–1369 (1994).
3. R. D. Watson, F. M. Hosking, M. F. Smith and C. D. Croessmann, Development and testing of the ITER divertor monoblock braze design, *Fusion Technol.* **19**, 1794–1798 (1991).
4. I. Smid, C. D. Croessmann, R. D. Watson, J. Linke, A Cardella, H. Bolt, N. Reheis and E. Kny, Performance of brazed graphite, carbon-fiber composite, and TZM materials for actively cooled structures: qualifications tests, *Fusion Technol.* **19**, 2035–2040 (1991).
5. S. Deschka, M. Akiba, G. Breitbach, A. Cardella, J. Linke, H. Nickel and N. Reheis, Thermal response and fatigue behaviour of brazed CFC/TZM/Mo41Re-divertor mock-ups under electron beam loading, *Proceedings of the 17th Symposium on Fusion Technology*, pp. 247–251, Rome (1992).
6. M. Araki, M. Akiba, M. Sugihara, S. Suzuki, S. Nishio and K. Yokoyama, Analytical and experimental evaluations of simulated sweeping heat load on the divertor plate for ITER, *Fusion Engng Design* **22**, 217–227 (1993).
7. T. Hino and T. Yamashina, Evaluation for boron mixed graphite and high Z metal as plasma facing material, *J. Nucl. Mater.* **196–198**, 531–536 (1992).
8. G. Janeschitz, A. Antipenkov, S. Chiocchio, J. Dietz, G. Federici *et al.*, The physics basis and design of the ITER divertor and of the pumping, fueling system, IAEA-CN-60/E-P-6, Seville, Spain (1994).
9. F. W. Dittus and L. M. K. Boelter, *Univ. Calif. Publs Engrs* **2**, 443 (1930).
10. W. H. Jens and P. A. Lottes, A.N.L. Report 4627 (1951).
11. W. R. Gambill, R. D. Bundy and R. W. Wansbrough, Report ORNL-2911, Oakridge National Laboratory (1960).
12. A. E. Bergles and W. M. Rohsenow, The determination of forced-convection surface-boiling heat transfer, *J. Heat Transfer* 365–372 (1964).
13. J. R. S. Thom, W. M. Walker, T. A. Fallon and G. F. S. Reising, Boiling in sub-cooled water during flow up heated tubes or annuli, *Proc. Instn Mech. Engrs* **80**(3C), 226–246 (1966).
14. M. M. Shah, Generalized prediction of heat transfer during subcooled boiling in annuli, *Heat Transfer Engng* **4**(1), 24–31 (1983).
15. J. Kim, R. C. Davis, W. R. Gambill and H. H. Haselton, A heat transfer study of water-cooled swirl tubes, *Proceedings of the Seventh Symposium on Engineering Problems of Fusion Research*, pp. 1593–1594, Knoxville, TN (1977).
16. S. L. Milora, S. K. Combs and C. A. Foster, A numerical model for swirl flow cooling in high-heat-flux particle beam targets and the design of a swirl-flow-based plasma limiter, *Nucl. Engng Design/Fusion* **3**, 301–308 (1986).
17. J. Schlosser and J. Boscary, Thermal-hydraulic tests at NET/ITER relevant conditions on divertor targets using swirl tubes, *Proceedings of NURETH-6*, pp. 815–824, Grenoble (1993).
18. M. Araki, M. Dairaku, T. Inoue, M. Komata, M. Kuriyama, S. Matsuda, M. Ogawa, Y. Ohara, M. Seki and K. Yokoyama, Burnout experiments on the externally-finned swirl tube for steady-state and high-heat flux beam stops, *Fusion Engng Design* **9**, 231–236 (1989).
19. S. Ikeda, M. Araki, M. Ogawa, M. Akiba and Y. Nishino, JAERI-M 893-070, Japan Atomic Energy Research Institute-report, (March 1993) (in Japanese) and also see M. Araki, M. Akiba, R. D. Watson, C. B. Baxi, D. L. Youchison, Data bases for thermo-hydrodynamic coupling with coolant, *Atomic Plasma-Material Interaction Processes in Controlled Thermonuclear Fusion* **5**, 245–265 (1995).
20. M. Araki, S. Ikeda, M. Ogawa, T. Kunugi, Y. Nishino, M. Akiba, K. Satoh, S. Suzuki, M. Dairaku, K. Nakamura and K. Yokoyama, JAERI-Tech 95–022, Japan Atomic Energy Research Institute (1995).
21. C. A. Brebbia, *The Boundary Element Method for Engineers*. Pentech Press Limited, London (1978).
22. S. T. Yin, Z. Jin, A. H. Abdelmessih and P. J. Gierszewski, Prediction of highly subcooled flow boiling for cooling of high heat-flux components in fusion reactors, *Proceedings of NURETH-6*, pp. 733–741, Grenoble (1993).